Spin-orbital order in $LaMnO_3$: $d-p$ model study

Krzysztof Rościszewski[1] and Andrzej M. Oleś[2,1]
[1]*Marian Smoluchowski Institute of Physics, Jagiellonian University, Prof. S. Łojasiewicza 11, PL-30348 Kraków, Poland*
[2]*Max Planck Institute for Solid State Research, Heisenbergstrasse 1, D-70569 Stuttgart, Germany*

(Received 13 February 2019; revised manuscript received 22 March 2019; published 3 April 2019)

Using the multiband $d-p$ model and unrestricted Hartree-Fock approximation, we investigate the electronic structure and spin-orbital order in three-dimensional MnO_3 lattice such as realized in $LaMnO_3$. The orbital order is induced and stabilized by particular checkerboard pattern of oxygen distortions arising from the Jahn-Teller effect in the presence of strong Coulomb interactions on e_g orbitals of Mn ions. We show that the spin-orbital order can be modeled using a simple *Ansatz* for local crystal fields alternating between two sublattices on Mn ions, which have nonequivalent neighboring oxygen distortions in *ab* planes. The simple and computationally very inexpensive $d-p$ model reproduces correctly nontrivial spin-orbital order observed in undoped $LaMnO_3$. Orbital order is very robust and is reduced by $\sim$3 % for large self-doping in the metallic regime.

DOI: 10.1103/PhysRevB.99.155108

I. INTRODUCTION

The spin and orbital ordering found in three dimensional $LaMnO_3$ perovskite is an old problem which is nowadays quite well understood [1,2], see also early and recent experimental and theoretical references [3–26]. The short summary and conclusions coming out from these papers are as follows. At zero temperature, the $LaMnO_3$ lattice has orthorhombic symmetry. The lattice is distorted due to strong Jahn-Teller (JT) effect: the MnO_6 octahedra are deformed, as shown schematically using the simplified picture for the *ab* ferromagnetic (FM) plane (nonzero tilting of the octahedra is neglected in this study) in Fig. 1. The magnetic moments on Mn ions correspond to spins $S \simeq 2$ and the magnetic structure is of the *A*-type antiferromagnetic (*A*-AF), i.e., FM order on separate *ab* planes, coupled antiferromagnetically plane-to-plane along the crystallographic *c* axis. The electron occupations on manganese t_{2g} orbitals $\{xy, yz, zx\}$ are very close to 1, while both e_g orbitals, $\{x^2-y^2, 3z^2-r^2\}$, contain together roughly one (the fourth) electron. The orbital order which settles in e_g orbitals is not seen when using the standard $\{x^2-y^2, 3z^2-r^2\}$ basis (which corresponds to choosing *z* quantization axis direction). However, if we consider a checkerboard pattern superimposed upon *ab* plane and choose *x* axis of quantization on "black" fields (MnO_4 rhombuses $m=2$ expanded along *x* axis, see Fig. 1), and *y* axis of quantization on "white" fields (MnO_4 rhombuses $m=1$ expanded along *y* axis), then the orbital order becomes transparent: the orbitals with majority electron occupations follow the $3x^2-r^2$ / $3y^2-r^2$ pattern. Oxygen distortions repeat along the *c* axis, and e_g orbitals follow. The common terminology to describe this type of order is *C*-type alternating orbital (*C*-AO) order.

The origin of the orbital order was under debate using effective $3d$ models taking into account electron-electron and electron-lattice interactions [17,27–30]. It was established that large JT splitting and superexchange are together responsible for *C*-AO order observed in $LaMnO_3$ [28–30]. Surprisingly, electron-lattice interaction is too weak to induce the orbital

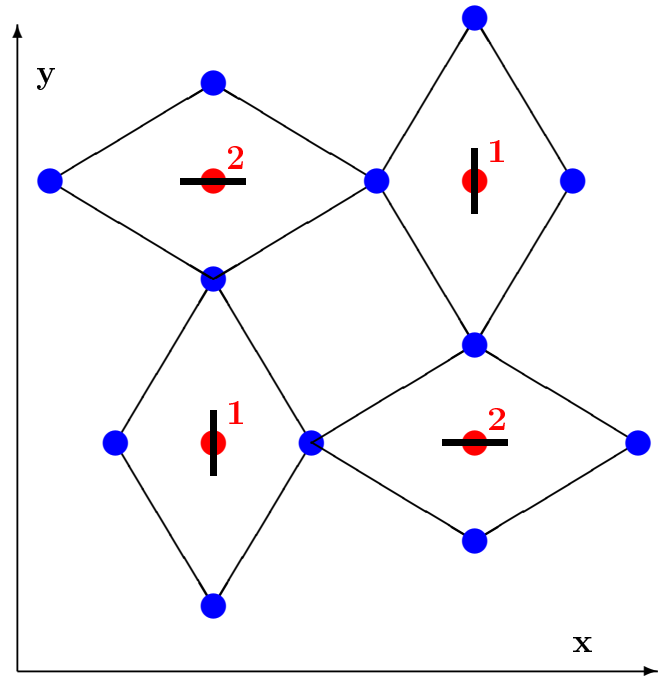

FIG. 1. Schematic view of JT distortions used for the Hartree-Fock (HF) computations. A single *ab* plane of the low-temperature phase of $LaMnO_3$ is presented. Red/blue dots denote positions of manganese/oxygen ions. The long bars denote energy-privileged (due to local crystal fields) $3y^2-r^2$ orbitals (at Mn_1) or $3x^2-r^2$ orbitals (at Mn_2 ions)—their cooperative arrangement corresponds to orbital order which supports FM spin order (spins are not shown). The numbers close to manganese positions identify different ions (see the corresponding entries in Table II) as belonging to $3y^2-r^2$ ($m=1$) and $3x^2-r^2$ ($m=2$) orbitals with lower energy. Note that horizontal and vertical directions on the figure correspond to *x* and *y* axes, respectively, which are at 45° angle to the crystallographic $\{a, b\}$ axes. Orbital order is repeated in consecutive layers along the *z* (crystallographic *c*) axis.

order alone and has to be helped by electron-electron superexchange [17]. Importance of the joint effect of strong correlations and Jahn-Teler distortions was concluded from the dynamical mean field theory [18]. On the other hand, superexchange alone would stabilize C-AO order but the order would be fragile and the orbital ordering temperature would be too low [29,31].

The large $S = 2$ spins at Mn^{3+} ions are coupled by spin-orbital superexchange which stabilizes A-AF spin order in $LaMnO_3$ below Néel temperature $T_N = 140$ K. However, spin order parameter could be little reduced if the *ideal ionic model* approximation does not strictly apply and the actual number of electrons transferred from La to MnO_3 subsystem is reduced to $3 - x$, i.e., one has $La^{+(3-x)}(MnO_3)^{-3+x}$, where x is so-called *self-doping*.

The idea of self-doping comes directly from *ab initio* computations and may be addressed when $d-p$ hybridization is explicitly included in the $d-p$ model. There, a rather trivial know-how is that charges on cations, computed using simple Mulliken population analysis—or better Bader population analysis—are almost never the same as in the idealized ionic model. Therefore, it is quite reasonable to introduce into the $d-p$ model the idea that each $La^{+(3-x)}$ donates onto MnO_3 lattice on average not 3 but $3 - x$ electrons. The self-doping can be regarded as a free parameter which could be adjusted using some additional experimental data. However, on the other hand, one can compute x using *ab initio* or density functional theory (DFT) with local Coulomb interaction U (DFT+U) cluster computations, exactly like it was done in Ref. [32]. This is, however, very costly, and contradicts one of the most important virtues of the $d-p$ model, i.e., time and cost efficiency of the computations.

Returning now to x in $LaMnO_3$, we note that if x is finite but still small enough, other magnetic phases could be more stable—in particular ordinary FM order is found frequently. Such a situation was studied experimentally in $Sr_xLa_{1-x}MnO_3$ [12]; note that here subscript x in the chemical formula $Sr_xLa_{1-x}MnO_3$ which routinely is identified as ordinary *doping* is only roughly similar to our *self-doping* x. When we increase ordinary doping x from very small towards intermediate values, then the metallic regime sets in $Sr_xLa_{1-x}MnO_3$ [2].

The purpose of this short paper is to investigate whether the spin-orbital order observed in $LaMnO_3$ would arise in the multiband $d-p$ model with the explicit treatment of oxygen $2p$ electrons. Here we focus on simple modeling of the JT effect, where oxygen distortions are treated as semiempirical input for the electronic $d-p$ model. To make the model realistic, we also include in it nonzero Coulomb repulsion on oxygen ions and spin-orbit interaction on Mn ions. Note that model studies done on $LaMnO_3$ before usually neglected these Hamiltonian components. In addition, we would like to account for the possibility of nontrivial self-doping $x \neq 0$ (just as found before in ruthenium, iridium, titanium, and vanadium oxides [33–35]).

The paper is organized as follows. We introduce the model Hamiltonian and its parameters in Sec. II. The numerical method is presented in Sec. III, where we treat the JT effect in a semiempirical way (Sec. III A), and present the unrestricted Hartree-Fock approximation in Sec. III B as a method of choice to describe the states with broken spin-orbital symmetries. It was shown recently that this approach gives very reliable results for doped vanadium perovskites [36]. The magnetization direction is there one of the open questions and we discuss possible states in Sec. III C. The ground state of $LaMnO_3$ is described in Secs. IV A, IV B, and IV C for three self-doping levels, $x = 0, 1/16$, and $1/8$. Finally, we also remark on the consequences of neglected e_g and t_{2g} splittings in Sec. IV D. In Sec. V, we present the dependence of orbital order parameter on the self-doping level and conclude that the order is robust. A short summary and conclusions are presented in Sec. VI.

II. HAMILTONIAN

We introduce the multiband $d-p$ Hamiltonian for MnO_3 three-dimensional $4 \times 4 \times 4$ (periodic boundary conditions) cluster which includes five $3d$ orbitals at each manganese ion and three $2p$ orbitals at each oxygen ion,

$$\mathcal{H} = H_{dp} + H_{pp} + H_{\rm so} + H_{\rm diag} + H^d_{\rm int} + H^p_{\rm int}, \tag{1}$$

where H_{dp} stands for the $d-p$ hybridization and H_{pp} for the interoxygen $p-p$ hopping, $H_{\rm so}$ is the spin-orbit coupling, $H_{\rm diag}$ is the diagonal part of kinetic energy (bare levels energies and local crystal fields). Here, $H^d_{\rm int}$ and $H^p_{\rm int}$ stand for the intraatomic Coulomb interactions at Mn and O ions, respectively. Optionally one could add JT energy as $H_{\rm JT}$. However, instead of introducing this term with a quite complicated form [37], we shall model the JT interaction by a simple *Ansatz* which can be inserted into $H_{\rm diag}$ as local potentials acting on e_g electrons. The cluster geometry and precise forms of different terms are standard; these terms were introduced in the previous realizations of the $d-p$ model devoted to transition metal oxides [33–35].

The kinetic energy in the Hamiltonian (1) consists of

$$H_{dp} = \sum_{\{m\alpha;j\nu\},\sigma} \left(t_{m\alpha;j\nu} d^\dagger_{m\alpha,\sigma} p_{j\nu,\sigma} + \text{H.c.}\right), \tag{2}$$

$$H_{pp} = \sum_{\{i\mu;j\nu\},\sigma} \left(t_{i\mu;j\nu} p^\dagger_{i\mu,\sigma} p_{j\nu,\sigma} + \text{H.c.}\right), \tag{3}$$

where $d^\dagger_{m\alpha,\sigma}$ ($p^\dagger_{j\nu,\sigma}$) is the creation operator of an electron at manganese site m (oxygen site j) in an orbital α (ν) with up or down spin, $\sigma = \uparrow, \downarrow$. The model includes all five $3d$ orbital states $\alpha \in \{xy, yz, zx, x^2 - y^2, 3z^2 - r^2\}$, and three $2p$ oxygen orbital states, $\{\mu, \nu\} \in \{p_x, p_y, p_z\}$. In the following we will use shorthand notation, and instead of $\{x^2 - y^2, 3z^2 - r^2\}$ we shall write $\{(\bar{z}), (z)\}$—this emphasizes the fact that z axis is chosen as the quantization axis for this e_g orbital basis, while () brackets are here to distinguish these Mn($3d$) orbitals from O($2p$) $\{x, y, z\}$ orbitals. The matrices $\{t_{m\alpha;j\nu}\}$ and $\{t_{i\mu;j\nu}\}$ are assumed to be nonzero only for nearest neighbor manganese–oxygen $d-p$ pairs, and for nearest neighbor oxygen–oxygen $p-p$ pairs. The next nearest neighbor hoppings are neglected. (The nonzero $\{t_{m\alpha;j\nu}\}$ and $\{t_{i\mu;j\nu}\}$ elements are listed in Appendix of Ref. [33]).

The spin-orbit part, $H_{\rm so} = \zeta \sum_i \mathbf{L}_i \cdot \mathbf{S}_i$, is a one-particle operator (scalar product of angular momentum and spin operators at site i), and it can be represented in the form similar

to the kinetic energy $H_{\rm kin}$ [38–41],

$$H_{\rm so} = \sum_m \left\{ \sum_{\alpha\neq\beta;\sigma,\sigma'} t^{so}_{\alpha,\sigma;\beta,\sigma'} d^\dagger_{m\alpha,\sigma} d_{m\beta,\sigma'} + \text{H.c.} \right\}, \quad (4)$$

with $t^{so}_{\alpha,\sigma;\beta,\sigma'}$ elements restricted to single manganese sites. They all depend on spin-orbit coupling strength ζ ($\zeta \approx 0.04$ eV [42]), which is weak but still it influences the preferred spin direction in the A-AF phase. For detailed formulas and tables listing $\{t^{so}_{\alpha,\sigma';\beta,\sigma}\}$ elements, see Refs. [33,39].

The diagonal part $H_{\rm diag}$ depends on electron number operators. It takes into account the effects of local crystal fields and the difference of reference orbital energies (here we employ the electron notation),

$$\Delta = \varepsilon_d - \varepsilon_p, \quad (5)$$

between d and p orbitals (for bare orbital energies) where ε_d is the average energy of all $3d$ orbitals, i.e., the reference energy before they split in the crystal field. We fix this reference energy for d orbitals to zero, $\varepsilon_d = 0$, and use only $\Delta = -\varepsilon_p$ and the crystal field splittings $\{f^{cr}_{m\alpha,\sigma}\}$ as parameters, thus we write

$$H_{\rm diag} = \sum_{i;\mu=x,y,z;\sigma} \varepsilon_p p^\dagger_{i\mu,\sigma} p_{i\mu,\sigma} + \sum_{m;\alpha=xy,yz,\ldots;\sigma} f^{cr}_{m\alpha,\sigma} d^\dagger_{m\alpha,\sigma} d_{m\alpha,\sigma}. \quad (6)$$

The first sum is restricted to oxygen sites $\{i\}$, while the second one runs over manganese sites $\{m\}$. The crystal-field splitting strength vector ($f^{cr}_{m\alpha,\sigma}$) describes the splitting within t_{2g} and within e_g levels, as well as the t_{2g} to e_g splitting, respectively.

Furthermore, the distance $10Dq$ between t_{2g} levels and e_g levels is ∼1.7 eV [43]). For the group of t_{2g} levels and their splittings in accordance with local JT distortion of particular MnO_6 octahedron *we assume* that either yz is lower than zx orbital, which should correspond to O_4 square (in ab plane) when distorted from an ideal square into rhombus elongated along y direction, or the opposite: zx is lower than yz orbital, which should correspond to O_4 distorted into rhombus elongated along x direction (compare Fig. 2). The splitting value should be ∼0.1 eV what is an educated guess (compare Ref. [35]) or even smaller [16]. What concerns the occupied e_g levels—they are also split. We assume varying (ion to ion) local crystal fields and choose appropriately the local axes of quantization, following Mn sublattices shown in Fig. 1.

In rhombuses elongated along the x axis (see Fig. 1), we use $3d$ orbital states at Mn sites $\{m\}$, $\{\alpha,\beta\} \in \{xy, yz, zx, y^2-z^2, 3x^2-r^2\}$ and correspondingly new $\{D^\dagger_{m\alpha,\sigma}\}$ creations operators; the new form of local crystal field is $f^{cr}_{m\alpha,\sigma} D^\dagger_{m\alpha,\sigma} D_{m\alpha,\sigma}$. Here our shorthand notation for $\{y^2-z^2, 3x^2-r^2\}$ orbitals will be $\{(\bar{x}),(x)\}$ (now x is chosen as the quantization axis). On the other hand, in rhombuses elongated along the y axis (see Fig. 1), we use the following $3d$ orbital states $\alpha \in \{xy, yz, zx, x^2-z^2, 3y^2-r^2\}$ and correspondingly new $\tilde{D}^\dagger_{m\alpha,\sigma}$ creation operators and the new form of local crystal field $f^{cr}_{m\alpha,\sigma} \tilde{D}^\dagger_{m\alpha,\sigma} \tilde{D}_{m\alpha,\sigma}$. Here our shorthand notation for $\{z^2-x^2, 3y^2-r^2\}$ orbitals is $\{(\bar{y}),(y)\}$ (now y is chosen as the quantization axis).

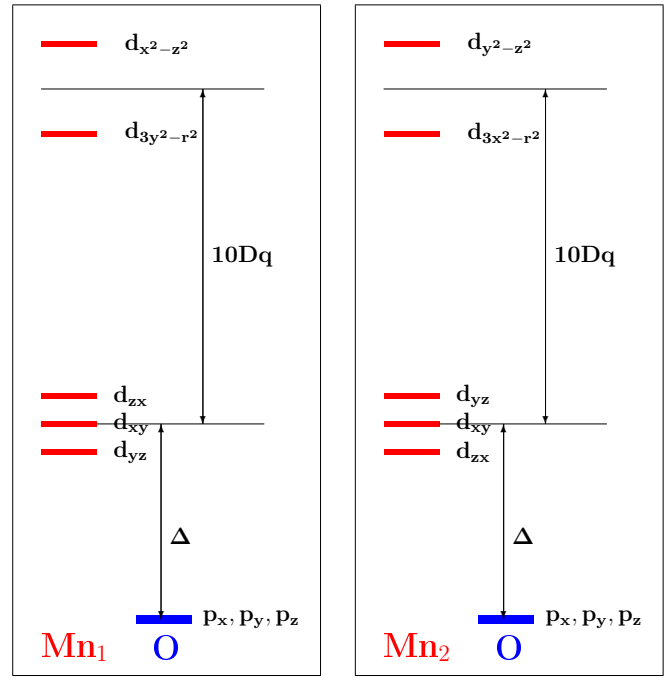

FIG. 2. Artist's view of the bare $3d$ levels (no interaction) at Mn_m ($m = 1, 2$) ions split by local crystal fields originating from JT distortions, $2p$ oxygen levels in the $d-p$ model. (a) Left: yz orbital is lower than zx orbital which corresponds to O_4 square when distorted from an ideal square into rhombus elongated along y direction (see Mn_1 ions in Fig. 1), e_g levels are also split—$3y^2-r^2$ is lower than x^2-z^2 (here y axis is chosen as the quantization axis). (b) Right: zx orbital is lower than yz orbital which corresponds to O_4 square when distorted from an ideal square into rhombus elongated along x direction (see Mn_2 ions in Fig. 1), e_g levels are also split—$3x^2-r^2$ is lower than y^2-z^2 (here x axis is chosen as the quantization axis). The average distance between t_{2g} levels and e_g levels ($10Dq$) is ∼1.7 eV [43], and Δ is oxygen-to-manganese charge-transfer energy.

Returning now to rhombuses expanded along the x axis when we work with $D^\dagger_{(x)\sigma}$ and $D^\dagger_{(\bar{x})\sigma}$ operators (x quantization axis) the corresponding canonical transformation is

$$\begin{pmatrix} D^\dagger_{(\bar{x})\sigma} \\ D^\dagger_{(x)\sigma} \end{pmatrix} = \begin{pmatrix} -\frac{1}{2} & -\frac{\sqrt{3}}{2} \\ \frac{\sqrt{3}}{2} & -\frac{1}{2} \end{pmatrix} \begin{pmatrix} d^\dagger_{(\bar{z})\sigma} \\ d^\dagger_{(z)\sigma} \end{pmatrix}, \quad (7)$$

where d operators are standard (i.e., for the z quantization axis).

We can also compute the operators of particle numbers, which are

$$D^\dagger_{(\bar{x})\sigma} D_{(\bar{x})\sigma} = \frac{1}{4} d^\dagger_{(\bar{z})\sigma} d_{(\bar{z})\sigma} + \frac{3}{4} d^\dagger_{(z)\sigma} d_{(z)\sigma} + \frac{\sqrt{3}}{4} (d^\dagger_{(\bar{z})\sigma} d_{(z)\sigma} + d^\dagger_{(z)\sigma} d_{(\bar{z})\sigma}), \quad (8)$$

$$D^\dagger_{(x)\sigma} D_{(x)\sigma} = \frac{3}{4} d^\dagger_{(\bar{z})\sigma} d_{(\bar{z})\sigma} + \frac{1}{4} d^\dagger_{(z)\sigma} d_{(z)\sigma} - \frac{\sqrt{3}}{4} (d^\dagger_{(\bar{z})\sigma} d_{(z)\sigma} + d^\dagger_{(z)\sigma} d_{(\bar{z})\sigma}). \quad (9)$$

Note that orbitals t_{2g} remain the same as before, i.e., they were not transformed.

When looking at the formulas just above we immediately see that while in $H_{\rm diag}$ the part with local crystal field is formally expressed by using $f^{cr}_{m\alpha,\sigma} D^{\dagger}_{m\alpha,\sigma} D_{m\alpha,\sigma}$, then in fact, thanks to Eqs. (8) and (9) we can still work with old standard d operators (z quantization axis).

Returning to rhombuses expanded along the y axis, we should work with $\tilde{D}^{\dagger}_{(\bar{y})\sigma}$ and $\tilde{D}^{\dagger}_{(y)\sigma}$ operators (for y quantization axis) and the corresponding formulas are

$$\begin{pmatrix} \tilde{D}^{\dagger}_{(\bar{y})\sigma} \\ \tilde{D}^{\dagger}_{(y)\sigma} \end{pmatrix} = \begin{pmatrix} \frac{1}{2} & -\frac{\sqrt{3}}{2} \\ -\frac{\sqrt{3}}{2} & -\frac{1}{2} \end{pmatrix} \begin{pmatrix} d^{\dagger}_{(\bar{z})\sigma} \\ d^{\dagger}_{(z)\sigma} \end{pmatrix}. \tag{10}$$

The particle number operators are

$$\tilde{D}^{\dagger}_{(\bar{y})\sigma} \tilde{D}_{(\bar{y})\sigma} = \frac{1}{4} d^{\dagger}_{(\bar{z})\sigma} d_{(\bar{z})\sigma} + \frac{3}{4} d^{\dagger}_{(z)\sigma} d_{(z)\sigma} - \frac{\sqrt{3}}{4} (d^{\dagger}_{(\bar{z})\sigma} d_{(z)\sigma} + d^{\dagger}_{(z)\sigma} d_{(\bar{z})\sigma}), \tag{11}$$

$$\tilde{D}^{\dagger}_{(y)\sigma} \tilde{D}_{(y)\sigma} = \frac{3}{4} d^{\dagger}_{(\bar{z})\sigma} d_{(\bar{z})\sigma} + \frac{1}{4} d^{\dagger}_{(z)\sigma} d_{(z)\sigma} + \frac{\sqrt{3}}{4} (d^{\dagger}_{(\bar{z})\sigma} d_{(z)\sigma} + d^{\dagger}_{(z)\sigma} d_{(\bar{z})\sigma}). \tag{12}$$

To make a short summary: the subsequent HF computations will be performed in the framework of the standard basis (i.e., old basis with z quantization axis) and after reaching self-consistency, we extract occupation numbers using formulas from Eqs. (8) and (9); to give an example the electron occupation in $3x^2 - r^2$ orbitals is just

$$\langle D^{\dagger}_{(x)\sigma} D_{(x)\sigma} \rangle = \frac{3}{4} \langle d^{\dagger}_{(\bar{z})\sigma} d_{(\bar{z})\sigma} \rangle + \frac{1}{4} \langle d^{\dagger}_{(z)\sigma} d_{(z)\sigma} \rangle - \frac{\sqrt{3}}{4} \langle d^{\dagger}_{(\bar{z})\sigma} d_{(z)\sigma} + d^{\dagger}_{(z)\sigma} d_{(\bar{z})\sigma} \rangle, \tag{13}$$

etc.

The on-site Coulomb interactions $H^{d}_{\rm int}$ for d orbitals take the form of a degenerate Hubbard model [44]

$$H^{d}_{\rm int} = \sum_{m,\alpha<\beta} \left(U_d - \frac{5}{2} J^{d}_{\alpha\beta} \right) n_{m\alpha} n_{m\beta} + U_d \sum_{m\alpha} n_{m\alpha,\uparrow} n_{m\alpha,\downarrow} - 2 \sum_{m,\alpha<\beta} J^{d}_{\alpha\beta} \vec{S}_{m\alpha} \cdot \vec{S}_{m\beta} + \sum_{m,\alpha\neq\beta} J^{d}_{\alpha\beta} d^{\dagger}_{m\alpha,\uparrow} d^{\dagger}_{m\alpha,\downarrow} d_{m\beta,\downarrow} d_{m\beta,\uparrow}, \tag{14}$$

where $n_{m\alpha} = \sum_{\sigma} n_{m\alpha,\sigma}$ is the electron density operator in orbital α; $\{\alpha, \beta\}$ enumerate different d orbitals, and $J_{d,\alpha\beta}$ is the tensor of on-site interorbital exchange (Hund's) elements for d orbitals; $J^{d}_{\alpha\beta}$ has different entries for the $\{\alpha, \beta\}$ pairs corresponding to two t_{2g} orbitals ($J^{t}_{\rm H}$), and for a pair of two e_g orbitals ($J^{e}_{\rm H}$), and still different for the case of cross-symmetry terms [31,45]; all these elements are included and we assume the Racah parameters: $B = 0.1$ eV and $C = 4B$.

TABLE I. Parameters of the multiband model (1) (all in eV) used in HF calculations. For the hopping integrals, we adopt the values from Refs. [6,38] and include oxygen-oxygen hopping elements in H_{pp}, given by $(pp\sigma) = 0.6$, $(pp\pi) = -0.15$ eV (here we use the Slater notation [50]). The charge-transfer energy Δ (5) is defined for bare levels. The magnitude of splitting within t_{2g} and e_g levels is arbitrarily taken as 0.1 eV and 0.2 eV.

ζ	$(pd\sigma)$	$(pd\pi)$	Δ	U_d	$J^{t}_{\rm H}$	$J^{e}_{\rm H}$	U_p	$J^{p}_{\rm H}$
0.04	−1.8	0.9	2.0	8.0	0.8	0.9	4.4	0.8

The local Coulomb interactions $H^{p}_{\rm int}$ at oxygen sites (for $2p$ orbitals) are analogous,

$$H^{p}_{\rm int} = \sum_{i,\mu<\nu,\sigma} \left(U_p - \frac{5}{2} J^{p}_{\rm H} \right) n_{i\mu} n_{i\nu} + U_p \sum_{i\mu} n_{i\mu,\uparrow} n_{i\mu,\downarrow} - 2 J^{p}_{\rm H} \sum_{i,\mu<\nu} \vec{S}_{i\mu} \cdot \vec{S}_{i\nu} + J^{p}_{\rm H} \sum_{i,\mu\neq\nu} p^{\dagger}_{i\mu\uparrow} p^{\dagger}_{i\mu\downarrow} p_{i\nu\downarrow} p_{i\nu\uparrow}, \tag{15}$$

where the intraatomic Coulomb repulsion is denoted as U_p and all off-diagonal elements of the tensor $J^{p}_{\mu\nu}$ are equal (as they connect the orbitals of the same symmetry), i.e., $J^{p}_{\mu\nu} \equiv J^{p}_{\rm H}$. Up to now, interaction at oxygen ions $H^{p}_{\rm int}$ were neglected in the majority of studies (i.e., for simplicity, it was being assumed that $U_p = J^{p}_{\rm H} = 0$).

In the following, we use the parameters U_d, $J^{d}_{\mu\nu}$, U_p, and $J^{p}_{\rm H}$ similar to those used before for titanium and vanadium oxides [34,35]; for the hopping integrals we follow the work by Mizokawa and Fujimori [6,38]. The value $U_p \sim 4.0$ eV was previously used in copper oxides [46,47]. Concerning the parameter Δ an educated guess is necessary. Old-fashioned computations, such as those reported in the classical textbook of Harrison [48] and shown in tables therein suggest 1.5 eV. Results of a more detailed study suggest that $\Delta < 2.5$ eV [49]. We also use the Slater notation [50]. We performed our computations for the parameter set in Table I.

Our reference system is $LaMnO_3$ where the total electron number in the $d-p$ subsystem is $N_e = 18 + 4 = 22$ per one MnO_3 unit provided we assume an ideal ionic model with no self-doping ($x = 0$), i.e., all three La valence electrons are transferred to MnO_3 unit. Another possibility is to take finite but small self-doping x. The problem how to fix x is a difficult question. The best way is to perform independent, auxiliary *ab initio* or local density approximation (LDA) with Coulomb interaction U (LDA+U) computations and to extract the electronic population on the cation R (in $RMnO_3$) analogously like it was done in Ref. [32]. This is however quite expensive. Without such auxiliary *ab initio* computations one is left either with speculations or one should perform computations using several different values of x.

III. NUMERICAL STUDIES

A. Computational problems concerning the Jahn-Teller Hamiltonian

Now let us return once more to the important part of the electronic Hamiltonian in perovskites, namely to the influence of JT distortions on the electronic structure. These rarely can be treated in a direct (and exact) way during the computations. Most often a semiempirical treatment of JT terms is used: namely, one assumes an explicit form and the magnitudes of the lattice distortions, such as suggested by experiments. Thus the distorted lattice is frozen and we take this as the experimental fact. The JT modes and the JT Hamiltonian do not enter computations anymore—their only role is to deform the lattice and to change Mn–O distances. Instead, one collects all Mn–O and O–O bond lengths (as suggested by experiment) and because of modified bond lengths one modifies the matrix of kinetic hopping parameters. In this respect, quite popular is the Harrison scaling [48]. We have used it in the present study.

The second important consequence of changed Mn–O distances is the creation of additional local crystal fields (in addition to standard crystal field which is responsible for t_{2g} to e_g splitting). These additional local crystal fields renormalise bare energy levels within e_g doublets and within t_{2g} triplets. (Note that this picture is valid at the level of static one-particle effective-potential approximation; i.e., it is similar like crystal-field cubic potential approximation which gives rise to standard $10Dq$ splitting). Thus, as the second part of modeling JT effect, what we do is the following: e_g doublets and t_{2g} triplets will be split as already discussed (in the previous section) for $H_{\rm diag}$ and $f^{cr}_{m\alpha,\sigma}$.

B. Unrestricted Hartree-Fock computations

We use the unrestricted HF approximation (UHF) (with a single determinant wave function) to investigate the $d-p$ model (1). The technical implementation is the same as that described in Refs. [6,33,34,38] featuring the averages $\langle d^{\dagger}_{m\alpha,\uparrow} d_{m\alpha,\uparrow}\rangle$ and $\langle p^{\dagger}_{i\mu,\uparrow} p_{i\mu,\uparrow}\rangle$ (in the HF Hamiltonian) which are treated as order parameters. We use the $4\times4\times4$ clusters which are sufficient for the present $d-p$ model with only nearest-neighbor hopping terms. During HF iterations the order parameters are recalculated self-consistently until convergence. The studied scenarios for the ground-state symmetry were those with spin order: FM, A-AF, G-AF (Néel state), C-AF (AF in ab plane, repeated in the consecutive ab planes when moving along the c axis), or nonmagnetic; the considered easy magnetization direction was either x or z.

To improve HF-convergence we used the quantum chemistry technique called level shifting [51]. It is based on replacing the true HF Hamiltonian by a different Hamiltonian—the one with the identical eigenvectors (one particle eigenfunctions) as the original Hamiltonian and with identical *occupied* eigenenergies. The original eigenenergies of virtual states are however uniformly shifted upwards by a fixed constant value. When applying virtual level shifting we can obtain some additional information. Namely when the splitting between the highest occupied molecular orbital (HOMO) and the lowest unoccupied molecular orbital (LUMO), i.e., HOMO-LUMO splitting (after correcting for the shift) is negative or zero, then the single-determinant HF ground state we obtained is not correct and usually the reason is that the true ground state is in fact conducting. We remind that the HOMO-LUMO gap serves here as an estimate of the experimental band gap.

TABLE II. Spin-orbital order and electron densities $\langle n_{m\alpha}\rangle$ obtained on nonequivalent Mn ions for the HF ground state (at zero temperature) as obtained for orthorhombic $LaMnO_3$ at self-doping $x=0$ and 0.0625. The index $m=1,2$ denotes a Mn site of a given sublattice, as shown in Fig. 1. Numbers in bold indicate the most appropriate quantization direction, i.e., the best local orbital basis for the description of orbital order at a given sublattice. The HF calculations are summarized by: the HF energy per MnO_3 unit cell, $E_{\rm HF}$, and the HOMO-LUMO gap G.

self-doping	***A*-AF / *C*-AO spin-orbital order**			
x	0		0.0625	
$E_{\rm HF}$ (eV)	123.507		122.156	
G (eV)	4.76		0.23	
	Mn ion sublattice			
electron density	$m=1$	$m=2$	$m=1$	$m=2$
$\langle n_{m,xy}\rangle$	1.02	1.02	1.02	1.02
$\langle n_{m,yz}\rangle$	1.00	1.02	1.00	1.02
$\langle n_{m,zx}\rangle$	1.02	1.00	1.02	1.00
$\langle n_{m,x^2-z^2}\rangle$	**0.12**	0.88	**0.11**	0.80
$\langle n_{m,3y^2-r^2}\rangle$	**1.00**	0.24	**0.95**	0.27
$\langle n_{m,y^2-z^2}\rangle$	0.89	**0.12**	0.81	**0.11**
$\langle n_{m,3x^2-r^2}\rangle$	0.23	**1.00**	0.26	**0.96**
$\langle n_{m,x^2-y^2}\rangle$	0.67	0.68	0.68	0.69
$\langle n_{m,3z^2-r^2}\rangle$	0.45	0.44	0.39	0.37

C. Searching for the magnetization direction

We performed computations for several values of self-doping x. They give the orbital order for e_g orbitals of C-type alternating orbital (C-AO) order in the regime of low self-doping $x<\frac{1}{8}$ (see Table II). At the same time, the spin order is A-AF, with the easy-axis of magnetization along the x direction. The preferred spin direction is however not generic as the ground states with z easy axis and with x easy axis are almost degenerate (within accuracy below 1 meV). Average spin values on Mn ions are very close to $S=2$ and the HOMO-LUMO gaps G were also computed, see Table II.

Finally, we remark on the magnetic state obtained in HF calculations; the up- and down-spin occupations are equal, i.e., $\langle d^{\dagger}_{m\alpha,\uparrow} d_{m\alpha,\uparrow}\rangle = \langle d^{\dagger}_{m\alpha,\downarrow} d_{m\alpha,\downarrow}\rangle$, thus the average zth spin component vanishes. However, this does not imply that the found ground states are nonmagnetic. We have found that the symmetry breaking with magnetization along x or y axis is equivalent, and the averages of the type, $\langle d^{\dagger}_{m\alpha,\uparrow} d_{m\alpha,\downarrow}\rangle$, are finite (not shown, but it is always the case for the data in Sec. IV). When the summation over μ is performed, i.e., if we calculate $Re\{\sum_{\alpha}\langle d^{\dagger}_{m\alpha,\uparrow} d_{m\alpha,\downarrow}\rangle\}$, we obtain the average spin component along the x direction, $|\langle S^x\rangle|$. This provides evidence that the spins are indeed aligned along the x axis, and we give the average magnetization $|\langle S^x\rangle|$ in Sec. V. The imaginary part of the same sum (if finite) does correspond to the average spin component along the y direction.

IV. GROUND STATE OF $LaMnO_3$

A. Zero self-doping $x = 0$

The ground state of $LaMnO_3$ has C-AO orbital order, and this is reproduced by the UHF calculations, see Table II, densities given in boldface. Note that when using only the standard orbital basis (i.e., the orbitals corresponding to the z quantization axis), the orbital order is completely hidden. To get more insightful results and to describe the orbital order induced by lattice distortions, we considered all the types of O_4 rhombuses.

It is important to realize that orbital order may be easily detected only for properly selected orbitals, depending on the sublattice. First, if the standard basis $\{3z^2 - r^2, x^2 - y^2\}$ is used, no trace of any orbital order is seen, see Table II. For the other two possible e_g bases, $\{3x^2 - r^2, y^2 - z^2\}$ and $\{3y^2 - r^2, z^2 - y^2\}$, one finds that the directional orbital has large electron density only on one sublattice, but on the other sublattice this is not the case. In other words, if one selects the x quantization axis, the orbital order is easily visible through a distinct asymmetry between Mn ions at this and the other sublattice, i.e., in positions $m = 1$ and $m = 2$, see Fig. 1. Thus the found asymmetry in the density distribution indicates that the order is of checkerboard type. Indeed, the checkerboard pattern of oxygen distortions requires choosing different local bases at two sublattices: on one with x quantization axis, and with y quantization axis on the other. Then the orbital order is clearly visible and the symmetry is correctly recovered, see the electron densities listed in boldface in Table II.

The spin order coexisting with C-AO order is A-AF, with the easy axis of magnetization along the x (y) direction, see Table II. Note that the state with the same characteristics but with easy magnetization axis along the z direction (not shown in Table II) is only by 0.3 meV higher (thus these two states are almost degenerate). The other HF states with C-AO order and with ordinary FM spin order are by 2 meV higher, while the states with G-AF or C-AF spin order are by 3.5 meV higher than the ground state. Nonmagnetic state is never realized.

With these results for the electron distribution, one could say that the experimental facts are faithfully reproduced. However, it is not so, as the HOMO-LUMO gap G we obtained is 4.76 eV, much larger than the experimentally measured; the experimental data concerning band gap are in the range of 1.1–1.7 eV (direct gap) [3,4,9] and 0.24 eV [5] (indirect gap). In fact, the HOMO-LUMO gap should correspond either to direct or to indirect gap, whichever is smaller. Anyway, for these both possibilities this discrepancy is by far too large and it invites one to reject thinking in terms of ideal-ionic model and to consider instead nonzero self-doping x. Note that our cluster is rather small thus we can not (in the following) consider and study any arbitrary value of self-doping x as this would in some cases result in noninteger electron number (in the cluster), and is some other case would result in an open-shell system (and such systems can not represent the ground state of an infinite crystal).

The density distribution found without self-doping (at $x = 0$) suggests that there is some but rather small electron transfer from O($2p$) to Mn($3d$) orbitals, see Table II. Indeed, we have verified that the electron density in all oxygen p orbitals is very close to 6.0, thus we deal with an almost "perfect" ionic system with O^{-2} ions.

B. Weak self-doping $x = 1/16$

The first possible close shell configuration is obtained by subtracting only four electrons from the total electron number in the $4 \times 4 \times 4$ cluster with $N_{\rm el} = 1408$ electrons at $x = 0$. In this case, we obtain the orbital order and spin order virtually the same as for $x = 0$ case (compare the density distribution for $x = 0$ and $x = 0.0625$ in Table II). However, total electron density in e_g orbitals is reduced by self-doping, see Table II. However, most importantly, the HOMO-LUMO gap G becomes much reduced to 0.23 eV, in satisfactory (though probably incidental) agreement with the experimental results [5].

Once again, one finds the ground state with the x quantization axis for the magnetization, and the complementary A-AF phase with the z easy spin direction is by 1.5 meV higher (per one unit cell). Other magnetic states are less favorable. The state with FM order is only by 2.0 meV higher, and the states with G-AF and C-AF spin order are both by ∼26 meV higher than the ground state. This result is important and reflects the proximity of the FM order in doped systems, which can be stabilized at still higher doping $x \sim 0.17$, as known from the phase diagram [52]. In fact, in the A-AF ground state the exchange interactions in ab planes are FM, and the described change of spin order involves just the change of sign of the exchange interaction along the c axis, from AF to FM.

C. Moderate self-doping: $x = 1/8$

Computations for $x \geqslant 1/8$ invariably produce the states with zero (or negative) HOMO-LUMO gaps. This can serve as an indication that the FM metallic regime sets in already at this self-doping level in the cluster under consideration.

Note that the experimental results for $La_{1-x}Sr_xMnO_3$ systems indicate that such systems are conducting and FM for $x > 0.2$ doping [52]. If we roughly identify our theoretical value of self-doping $x = 1/8 \approx 0.12$ with the doping by Sr, we approach the metallic regime, even when this value of x does not coincide yet with the experimental doping in metallic FM manganites ($x \sim 0.17$) [11,12]. We remark that such a discrepancy for small (not infinite) cluster and for simple empirical $d-p$ model can be expected.

D. Neglecting splitting within e_g and t_{2g} states

As already discussed, the modeling of JT Hamiltonian goes in two separate steps: (i) changing the bare energies of individual orbitals, and (ii) performing Harrison [48] scaling of hopping integrals due to modified Mn-O bond lengths [26], i.e., changing simultaneously static crystal-field potential and changing the kinetic part. To the best of our knowledge, only the second step (ii) is discussed in the literature.

Therefore (to conform to the main stream) we performed auxiliary computations putting to zero bare level splittings within e_g and t_{2g} multiplets but performing Harrison scaling to adjust the values of $d-p$ hopping elements to the actual bond lengths. It could appear surprising, but the results concerning the ground states did not change much. The magnetic order

and orbital order persist, albeit the orbital order is somewhat weaker. Thus it seems that the change which the JT effect brings upon kinetic Hamiltonian part (hopping elements) is the dominant change or at least it is just enough for a satisfactory modeling of the JT effect.

V. ROBUSTNESS OF ORBITAL ORDER

Finally, we address the question of stability of orbital order under self-doping. In doped manganites orbital order persists at low doping up to $x \simeq 0.1$ [2], and at higher doping orbital liquid [53] takes over which supports FM metallic phase. A remarkable feature of the perovskite vanadates is that orbital order is quite robust [54,55] and is destroyed only at high concentration of charged defects $x \simeq 0.20$ by orbital polarization interactions which frustrates orbital order [56].

To investigate orbital order and its dependence on self-doping x, we take $N_e = 64 \times (22 - x)$ electrons for $(4\times4\times4)$ cluster. Having in mind the charge distribution anisotropy in distorted rhombuses in ab planes, we define orbital order parameter $\eta_{y/x}$ for the observed C-AO order as follows:

$$2\eta_{y/x} = \frac{-\langle n_{1,x^2-z^2}\rangle + \langle n_{1,3y^2-r^2}\rangle}{\langle n_{1,x^2-z^2}\rangle + \langle n_{1,3y^2-r^2}\rangle} + \frac{-\langle n_{2,y^2-z^2}\rangle + \langle n_{2,3x^2-r^2}\rangle}{\langle n_{2,y^2-z^2}\rangle + \langle n_{2,3x^2-r^2}\rangle}, \tag{16}$$

where the electron densities appropriate to y/x quantization directions [as applied to $(m = 1)$ / $(m = 2)$ rhombuses; see Fig. 1] are used.

Once again we stress that when only one z-quantization direction (on all rhombuses) is used, then the C-AO orbital order is not visible at all. To make this picture complete we can define ordinary order parameter η_z as well,

$$2\eta_z = \frac{-\langle n_{1,x^2-y^2}\rangle + \langle n_{1,3z^2-r^2}\rangle}{\langle n_{1,x^2-y^2}\rangle + \langle n_{1,3z^2-r^2}\rangle} + \frac{-\langle n_{2,x^2-y^2}\rangle + \langle n_{2,3z^2-r^2}\rangle}{\langle n_{2,x^2-y^2}\rangle + \langle n_{2,3z^2-r^2}\rangle}, \tag{17}$$

which only shows the difference between electron densities $\langle n_{m,x^2-y^2}\rangle$ and $\langle n_{m,3z^2-r^2}\rangle$, (influenced by z-direction tetragonal distortion) which is *independent* of m, i.e., they are the same for $(m = 1)$-type and for $(m = 2)$-type rhombuses. We remark that sometimes one finds a tiny site-to-site charge modulation which is possibly an artifact due to imperfect convergence, we neglect it—to get rid of it in Eq. (17) we average η_z over $m = 1$ and $m = 2$ rhombuses.

The C-AO order parameter (16) versus hypothetical values of x (self-doping) is shown in Table III. It is very robust and almost independent of self-doping x up to rather high value $x = 3/16$. It is remarkable that C-AO order survives in the metallic regime at $x = 2/16$ and $x = 3/16$. On the contrary, the parameter η_z (17) is inconclusive concerning C-AO order. Instead, it shows that the electron density in $x^2 - y^2$ orbitals is higher than the one in $3z^2 - r^2$, in agreement with the model including tetragonal distortions [26].

TABLE III. The HOMO-LUMO gap G, the average magnetization value $|\langle S^x\rangle|$, and the orbital order parameters, $\eta_{y/x}$ and η_z, vs hypothetical values of self-doping x for $LaMnO_3$. All the presented data correspond to ground states characterized by coexisting A-AF spin (with x easy axis of magnetization) and C-AO order.

x	G (eV)	$\lvert\langle S^x\rangle\rvert$	$\eta_{y/x}$	η_z
0	4.76	1.98	0.79	−0.20
1/16	0.23	1.95	0.79	−0.28
2/16	≃0	1.92	0.78	−0.32
3/16	≃0	1.89	0.77	−0.35

VI. SUMMARY AND CONCLUSIONS

We have shown that the $d-p$ model with strong electron interactions reproduces correctly spin-orbital order in $LaMnO_3$, provided the electronic configuration of Mn ions is very close to Mn^{3+} and the oxygen distortions due to the Jahn-Teller effect are included. This implies also selecting the adequate orbital basis which is the most appropriate to describe the orbital ordered state stabilized by oxygen distortions. Thereby occupied e_g orbitals follow the oxygen distortions in ab planes, and one finds A-AF / C-AO order, as observed [1,52]. Similar to doped vanadium perovskites [56], our study shows that the spin-orbital order is here quite robust for low decrease of electron concentration in MnO_3 units.

We have shown that the self-doping in $LaMnO_3$ is small but finite and is in fact necessary to reproduce the observed insulating behavior with a small gap. This result emphasizes the importance of electronic charge delocalization over O($2p$) orbitals in the $d-p$ model for a charge-transfer insulator $LaMnO_3$.

This study completes the series of papers [33–35], where we have shown that the multiband $d-p$ model is capable of reproducing coexisting spin-orbital order in various situations and in various perovskites. In contrast to time-consuming *cluster ab initio* or LDA+U calculations [17–21], the computations using $d-p$ model are very efficient and should be regarded as easy and simple tool for any preliminary study to establish the electronic structure and ground state properties of an investigated perovskite. During such calculations the only difficult part is the proper choice of the Hamiltonian parameters. We suggest that this approach could be a promising technique to investigate heterostructures [57,58] or superlattices [59,60], where the Jahn-Teller effect plays an important role. On the other hand, when information about the correct values of Hamiltonian parameters are uncertain, one can perform computations with several sets of Hamiltonian parameters. The results of such computations when confronted with the experimental results could be eventually used for screening out wrongly chosen Hamiltonian parameter sets.

ACKNOWLEDGMENTS

We kindly acknowledge Narodowe Centrum Nauki (NCN, Poland) Project No. 2016/23/B/ST3/00839. A.M.O. is also grateful for the Alexander von Humboldt Foundation Fellowship (Humboldt-Forschungspreis).

[1] E. Dagotto, T. Hotta, and A. Moreo, Colossal Magnetoresistant Materials: The Key Role of Phase Separation, Phys. Rep. **344**, 1 (2001); E. Dagotto, Open Questions in CMR Manganites, Relevance of Clustered States and Analogies with Other Compounds Including the Cuprates, New J. Phys. **7**, 67 (2005).

[2] Y. Tokura, Critical features of colossal magnetoresistive manganites, Rep. Prog. Phys. **69**, 797 (2006).

[3] T. Arima, Y. Tokura, and J. B. Torrance, Variation of optical gaps in perovskite-type 3*d* transition-metal oxides, Phys. Rev. B **48**, 17006 (1993).

[4] T. Saitoh, A. E. Bocquet, T. Mizokawa, H. Namatame, A. Fujimori, M. Abbate, Y. Takeda, and M. Takano, Electronic structure of $La_{1-x}Sr_xMnO_3$ studied by photoemission and x-ray-absorption spectroscopy, Phys. Rev. B **51**, 13942 (1995).

[5] R. Mahendiran, A. K. Raychaudhuri, A. Chainini, D. Das Sarma, and S. B. Roy, Appl. Phys. Lett. **66**, 233 (1995).

[6] T. Mizokawa and A. Fujimori, Unrestricted Hartree-Fock study of transition-metal oxides: Spin and orbital ordering in perovskite-type lattice, Phys. Rev. B **51**, 12880 (1995).

[7] H. Sawada, Y. Morikawa, K. Terakura, and N. Hamada, Jahn-Teller distortion and magnetic structures in $LaMnO_3$, Phys. Rev. B **56**, 12154 (1997).

[8] M. Capone, D. Feinberg, and M. Grilli, Stabilization of *A*-type layered antiferromagnetic phase in $LaMnO_3$ by cooperative Jahn-Teller deformations, Eur. Phys. J. B **17**, 103 (2000).

[9] K. Tobe, T. Kimura, Y. Okimoto, and Y. Tokura, Anisotropic optical spectra in a detwinned $LaMnO_3$ crystal, Phys. Rev. B **64**, 184421 (2001).

[10] P. Ravindran, A. Kjekshus, H. Fjellvøag, A. Delin, and O. Eriksson, Ground-state and excited-state properties of $LaMnO_3$ from full-potential calculations, Phys. Rev. B **65**, 064445 (2002).

[11] Y. Endoh, K. Hirota, S. Ishihara, S. Okamoto, Y. Murakami, A. Nishizawa, T. Fukuda, H. Kimura, H. Nojiri, K. Kaneko, and S. Maekawa, Transition between Two Ferromagnetic States Driven by Orbital Ordering in $La_{0.88}Sr_{0.12}MnO_3$, Phys. Rev. Lett. **82**, 4328 (1999).

[12] D. Ivannikov, M. Biberacher, H.-A. Krug von Nidda, A. Pimenov, A. Loidl, A. A. Mukhin, and A. M. Balbashov, High-field ESR spectroscopy of the spin dynamics in $La_{1-x}Sr_xMnO_3$ ($x <\sim 0.175$), Phys. Rev. B **65**, 214422 (2002).

[13] M. Kataoka, Origin of the Antiferroorbital Ordering in $LaMnO_3$ and Other Related Compounds, J. Phys. Soc. Jpn. **73**, 1244 (2004).

[14] K. Ebata, T. Mizokawa, and A. Fujimori, Orbital ordering in $La_{0.5}Sr_{1.5}MnO_4$ studied by model Hartree-Fock calculation, Phys. Rev. B **72**, 233104 (2005).

[15] H. Zenia, G. A. Gehring, and W. M. Temmerman, Orbital ordering in cubic $LaMnO_3$ from first principles calculations, New J. Phys. **7**, 257 (2005).

[16] V. A. Gavrichkov, S. G. Ovchinnikov, and L. E. Yakimow, The role of orbital ordering in the formation of electron structure in undoped $LaMnO_3$ manganites in the regime of strong electron correlations, J. Exp. Theor. Phys. **102**, 972 (2006).

[17] W.-G. Yin, D. Volja, and W. Ku, Orbital Ordering in $LaMnO_3$: Electron-Electron versus Electron-Lattice Interactions, Phys. Rev. Lett. **96**, 116405 (2006).

[18] A. Yamasaki, M. Feldbacher, Y.-F. Yang, O. K. Andersen, and K. Held, Pressure-Induced Metal-Insulator Transition in $LaMnO_3$ Is Not of Mott-Hubbard Type, Phys. Rev. Lett. **96**, 166401 (2006).

[19] R. Kováčik and C. Ederer, Effect of Hubbard U on the construction of low-energy Hamiltonians for $LaMnO_3$ via maximally localized Wannier functions, Phys. Rev. B **84**, 075118 (2011).

[20] S. Gong and B.-G. Liu, Electronic energy gaps and optical properties of $LaMnO_3$, Phys. Lett. A **375**, 1477 (2011).

[21] T. A. Mellan, F. Cora, R. Grau-Crespo, and S. Ismail-Beigi, Importance of anisotropic Coulomb interaction in $LaMnO_3$, Phys. Rev. B **92**, 085151 (2015).

[22] E. Pavarini and E. Koch, Origin of Jahn-Teller Distortion and Orbital Order in $LaMnO_3$, Phys. Rev. Lett. **104**, 086402 (2010).

[23] N. N. Kovaleva, A. M. Oleś, A. M. Balbashov, A. Maljuk, D. N. Argyriou, G. Khaliullin, and B. Keimer, Low-energy Mott-Hubbard excitations in $LaMnO_3$ studied by optical spectroscopy, Phys. Rev. B **81**, 235130 (2010).

[24] A. L. Gavin and G. W. Watson, Defects in orthorhombic $LaMnO_3$—ionic versus electronic compensation, Solid State Ionics **299**, 13 (2017).

[25] S. W. Jang, S. Ryee, H. Yoon, and M. J. Han, Charge density functional plus U theory of $LaMnO_3$: Phase diagram, electronic structure, and magnetic interaction, Phys. Rev. B **98**, 125126 (2018).

[26] M. Snamina and A. M. Oleś, Spin-orbital model of stoichiometric $LaMnO_3$ with tetragonal distortions, Phys. Rev. B **97**, 104417 (2018).

[27] A. J. Millis, Orbital ordering and superexchange in manganite oxides, Phys. Rev. B **55**, 6405 (1997).

[28] D. Feinberg, P. Germain, M. Grilli, and G. Seibold, Joint superexchange-Jahn-Teller mechanism for layered antiferromagnetism in $LaMnO_3$, Phys. Rev. B **57**, R5583 (1998).

[29] L. F. Feiner and A. M. Oleś, Electronic origin of magnetic and orbital ordering in insulating $LaMnO_3$, Phys. Rev. B **59**, 3295 (1999).

[30] T. Hotta, S. Yunoki, M. Mayr, and E. Dagotto, *A*-type antiferromagnetic and *C*-type orbital-ordered states in $LaMnO_3$ using cooperative Jahn-Teller phonons, Phys. Rev. B **60**, R15009 (1999).

[31] A. M. Oleś, G. Khaliullin, P. Horsch, and L. F. Feiner, Fingerprints of spin-orbital physics in cubic Mott insulators: Magnetic exchange interactions and optical spectral weights, Phys. Rev. B **72**, 214431 (2005).

[32] K. Rościszewski, P. Piekarz, and A. M. Oleś, Multiband model for the Mott insulator Sr_2TiO_4, Phys. Stat. Sol. B **254**, 1700022 (2017); K. Rościszewski and A. M. Oleś, On the Neglect of Local Coulomb Interaction on Oxygens in Perovskites Described by the Multiband $d-p$ Model, Acta Phys. Polon. A **133**, 356 (2018).

[33] K. Rościszewski and A. M. Oleś, Charge transfer model for the electronic structure of layered ruthenates, Phys. Rev. B **91**, 155137 (2015).

[34] K. Rościszewski and A. M. Oleś, Multiband $d-p$ model and self-doping in the electronic structure of Ba_2IrO_4, Phys. Rev. B **93**, 085106 (2016).

[35] K. Rościszewski and A. M. Oleś, $d-p$ model and spin-orbital order in vanadium perovskites, Phys. Rev. B **98**, 085119 (2018).

[36] A. Avella, A. M. Oleś, and P. Horsch, Fingerprints of spin-orbital polarons and of their Disorder in the photoemission spectra of doped Mott insulators with orbital degeneracy, Phys. Rev. B **97**, 155104 (2018).

[37] K. A. Müller, *Jahn-Teller Effects in Magnetic Resonance*, in Properties of Perovskites and other Oxides, edited by K. A. Müller and T. W. Kool (World Scientific, Singapore, 2010).

[38] T. Mizokawa and A. Fujimori, Electronic structure and orbital ordering in perovskite-type 3*d* transition-metal oxides studied by Hartree-Fock band-structure calculations, Phys. Rev. B **54**, 5368 (1996).

[39] L. V. Poluyanov and W. Domcke, Development of multi-mode diabatic spin-orbit models at arbitrary order, J. Chem. Phys. **137**, 114101 (2012).

[40] H. Matsuura and K. Miyake, Effect of Spin-Orbit Interaction on $(4d)^3$- and $(5d)^3$-Based Transition-Metal Oxides, J. Phys. Soc. Jpn. **82**, 073703 (2013).

[41] L. Du, L. Huang, and X. Dai, Metal-insulator transition in three-band Hubbard model with strong spin-orbit interaction, Eur. Phys. J. B **86**, 94 (2013).

[42] D. Dai, H. Xiang, and M.-H. Whangbo, Effects of spin-orbit coupling on magnetic properties of discrete and extended magnetic systems, J. Comput. Chem. **29**, 2187 (2008).

[43] G. Zampieri, M. Abbate, F. Prado, A. Caneiro, and E. Morikawa, XPS and XAS spectra of $CaMnO_3$ and $LaMnO_3$, Physica B **320**, 51 (2002).

[44] A. M. Oleś, Antiferromagnetism and correlation of electrons in transition metals, Phys. Rev. B **28**, 327 (1983).

[45] P. Horsch, Orbital Physics in Transition-Metal Oxides: Magnetism and Optics, in *Handbook of Magnetism and Advanced Magnetic Materials*, edited by H. Kronmüller and S. Parkin, Volume 1: Fundamentals and Theory (Wiley, Hoboken, New York, 2007), p. 164.

[46] M. S. Hybertsen, E. P. Stechel, W. M. C. Foulkes, and M. Schluter, Model for low-energy electronic states probed by x-ray absorption in high-T_c cuprates, Phys. Rev. B **45**, 10032 (1992).

[47] *Electronic Structure and Magnetism of Complex Materials*, edited by D. J. Singh and D. A. Papaconstantopoulos, Springer Series in Material Science Vol. 54 (Springer, Berlin, Heidelberg, 2013).

[48] W. A. Harrison, *Elementary Electronic Structure* (World Scientific, London, 2005).

[49] R. Rauer, *Optical Spectroscopy of Strongly Correlated Transition Metal Oxides*, Ph.D. thesis, University of Hamburg, Cuvillier Verlag, Hamburg, 2005.

[50] C. Slater and G. F. Koster, Simplified LCAO Method for the Periodic Potential Problem, Phys. Rev. **94**, 1498 (1954).

[51] V. R. Sounders and I. H. Hillier, A "Level-Shifting" method for converging closed shell Hartree-Fock wave functions, Int. J. Quantum Chem. **7**, 699 (1973).

[52] A. Moreo, S. Yunoki, and E. Dagotto, Phase separation scenario for manganese oxides and related materials, Science **283**, 2034 (1999).

[53] L. F. Feiner and A. M. Oleś, Orbital liquid in ferromagnetic manganites: The orbital Hubbard model for e_g electrons, Phys. Rev. B **71**, 144422 (2005).

[54] S. Miyasaka, T. Okuda, and Y. Tokura, Critical Behavior of Metal-Insulator Transition in $La_{1-x}Sr_xVO_3$, Phys. Rev. Lett. **85**, 5388 (2000).

[55] J. Fujioka, S. Miyasaka, and Y. Tokura, Doping Variation of Orbitally Induced Anisotropy in the Electronic Structure of $La_{1-x}Sr_xVO_3$, Phys. Rev. Lett. **97**, 196401 (2006); Orbital disordering and the metal-insulator transition with hole doping in perovskite-type vanadium oxides, Phys. Rev. B **72**, 024460 (2005); Doping variation of anisotropic charge and orbital dynamics in $Y_{1-x}Ca_xVO_3$: Comparison with $La_{1-x}Sr_xVO_3$, *ibid.* **77**, 144402 (2008).

[56] A. Avella, A. M. Oleś, and P. Horsch, Defect-Induced Orbital Polarization and Collapse of Orbital Order in Doped Vanadium Perovskites, Phys. Rev. Lett. **122**, 127206 (2019).

[57] R. Yu, S. Yunoki, S. Dong, and E. Dagotto, Electronic and magnetic properties of $RMnO_3/AMnO_3$ heterostructures, Phys. Rev. B **80**, 125115 (2009).

[58] K. Rogdakis, J. W. Seo, Z. Viskadourakis, Y. Wang, L. F. N. Ah Qune, E. Choi, J. D. Burton, E. Y. Tsymbal, J. Lee, and C. Panagopoulos, Tunable ferroelectricity in artificial tri-layer superlattices comprised of non-ferroic components, Nat. Commun. **3**, 1064 (2012).

[59] D. Cao, M.-Q. Cai, W.-Yu Hu, J. Peng, Y. Zheng, and H.-T. Huang, Uniaxial strain-modulated conductivity in manganite superlattice ($LaMnO_3/SrMnO_3$), Appl. Phys. Lett. **98**, 031910 (2011).

[60] S. Dong, Q. Zhang, S. Yunoki, J.-M. Liu, and E. Dagotto, Magnetic and orbital order in $(RMnO_3)_n/(AMnO_3)_{2n}$ superlattices studied via a double-exchange model with strain, Phys. Rev. B **86**, 205121 (2012).